

Kinetic Characterization of Catalysis by the Chemotaxis Phosphatase CheZ

MODULATION OF ACTIVITY BY THE PHOSPHORYLATED CheY SUBSTRATE*

Received for publication, May 29, 2007, and in revised form, October 19, 2007. Published, JBC Papers in Press, November 12, 2007, DOI 10.1074/jbc.M704400200

Ruth E. Silversmith^{†1}, Matthew D. Levin^{§2}, Elmar Schilling^{†3}, and Robert B. Bourret[†]

From the [†]Department of Microbiology and Immunology, University of North Carolina, Chapel Hill, North Carolina 27599-7290

and [§]Department of Physiology, Development, and Neuroscience, University of Cambridge, Cambridge CB2 3EJ, United Kingdom

CheZ catalyzes the dephosphorylation of the response regulator CheY in the two-component regulatory system that mediates chemotaxis in *Escherichia coli*. CheZ is a homodimer with two active sites for dephosphorylation. To gain insight into cellular mechanisms for the precise regulation of intracellular phosphorylated CheY (CheYp) levels, we evaluated the kinetic properties of CheZ. The steady state rate of CheZ-mediated dephosphorylation of CheYp displayed marked sigmoidicity with respect to CheYp concentration and a k_{cat} of 4.9 s^{-1} . In contrast, the gain of function mutant CheZ-I21T with an amino acid substitution far from the active site gave hyperbolic kinetics and required far lower CheYp for half-saturation but had a similar k_{cat} value as the wild type enzyme. Stopped flow fluorescence measurements demonstrated a 6-fold faster CheZ/CheYp association rate for CheZ-I21T ($k_{\text{assoc}} = 3.4 \times 10^7 \text{ M}^{-1} \text{ s}^{-1}$) relative to wild type CheZ ($k_{\text{assoc}} = 5.6 \times 10^6 \text{ M}^{-1} \text{ s}^{-1}$). Dissociation of the CheZ-CheYBeF₃ complex was slow for both wild type CheZ ($k_{\text{dissoc}} = 0.040 \text{ s}^{-1}$) and CheZ-I21T ($k_{\text{dissoc}} = 0.023 \text{ s}^{-1}$) and, when taken with the k_{assoc} values, implied K_d values of 7.1 and 0.68 nM, respectively. However, comparison of the k_{dissoc} and k_{cat} values implied that CheZ and CheYp are not at binding equilibrium during catalysis and that once CheYp binds, it is almost always dephosphorylated. The rate constants were collated to formulate a kinetic model for CheZ-mediated dephosphorylation that includes autoregulation by CheYp and allowed prediction of CheZ activities at CheZ and CheYp concentrations likely to be present in cells.

In the two-component regulatory system that mediates chemotaxis in *Escherichia coli*, the cell continuously regulates the level of phosphorylation of the response regulator CheY in response to an external chemical gradient (1–4). Intracellular levels of phosphorylated CheY (CheYp)⁴ in turn directly dictate

cell swimming behavior. CheYp binds to the base of the flagellum, thereby changing the direction of flagellar rotation from counterclockwise (causing a forward run) to clockwise (causing a reorienting tumble). Because cells switch rapidly between these two swimming behaviors as they sample their environment (5, 6), it is essential that both phosphorylation and dephosphorylation of CheY occur on a rapid time scale so that the concentration of CheYp at any instant accurately reflects current environmental conditions. Moreover, the highly cooperative relationship between intracellular CheYp concentration and the probability of clockwise rotation (7) underscores the necessity of precise regulation of CheYp levels. CheY is phosphorylated on Asp-57 by its cognate sensor kinase CheA at a rate that is dictated by the rate of autophosphorylation of CheA with ATP, which in turn is a function of the activity state of coupled transmembrane receptors. CheYp is dephosphorylated by the phosphatase CheZ. The ability to perform chemotaxis is very sensitive to intracellular CheZ activity as either a modest increase or decrease of CheZ activity disables chemotaxis (8–12). Much of the cellular pool of CheZ is associated with the large polar signaling complex (13–15), which also contains receptors, CheA, and the scaffolding protein, CheW. Colocalization of CheZ with the CheA kinase implies some futile cycling of CheY but ensures a uniform concentration of CheYp across the length of the cell (15–17).

CheZ is unrelated by amino acid sequence to other known classes of protein phosphatases and has a unique catalytic mechanism based on the introduction of additional catalytic elements into the CheYp active site for CheYp autodephosphorylation activity. CheZ is a homodimer with two CheYp binding sites, each binding site being composed of two independent surfaces from different domains of CheZ₂ (Fig. 1 (18)). The dominant domain of CheZ₂ is a long four-helix bundle composed of a helical hairpin from each monomer with additional angled N-terminal helices at the non-hairpin end of the bundle. The C terminus of each hairpin extends with a 32-residue flexible linker followed by a final amphipathic C-terminal α helix (C-helix). Like all response regulators, CheY has a $\beta_5\alpha_5$ fold with the phosphorylated aspartate located within a highly conserved active site adjacent to a bound Mg²⁺ ion (19), essential for catalysis of all phosphotransfer events (20). In one interaction surface between CheY and CheZ, the $\alpha_4\beta_5\alpha_5$ surface of

* This work was supported by National Institutes of Health Grant GM 050860 (to R. B. B.). The costs of publication of this article were defrayed in part by the payment of page charges. This article must therefore be hereby marked "advertisement" in accordance with 18 U.S.C. Section 1734 solely to indicate this fact.

¹ To whom correspondence should be addressed. Tel.: 919-966-2679; Fax: 919-962-8103; E-mail: silversr@med.unc.edu.

² Supported by National Institutes of Health Grant GM 064713 (to D. Bray).

³ Current address: Dept. of Hematology and Oncology, Regensburg University Medical Center, Regensburg, 93042 Germany.

⁴ The abbreviations used are: CheYp, phosphorylated CheY; CheZ-I21T, isoleucine at position 21 changed to a threonine; *B-CheZ, CheZ-F214C with the badan fluorophore covalently linked to Cys-214; *B-CheZ-I21T, CheZ-

I21T/F214C with the badan fluorophore linked to Cys-214; MPI, mono-phosphoimidazole; CheYBeF₃, CheY with bound BeF₃⁻ and Mg²⁺ ions.

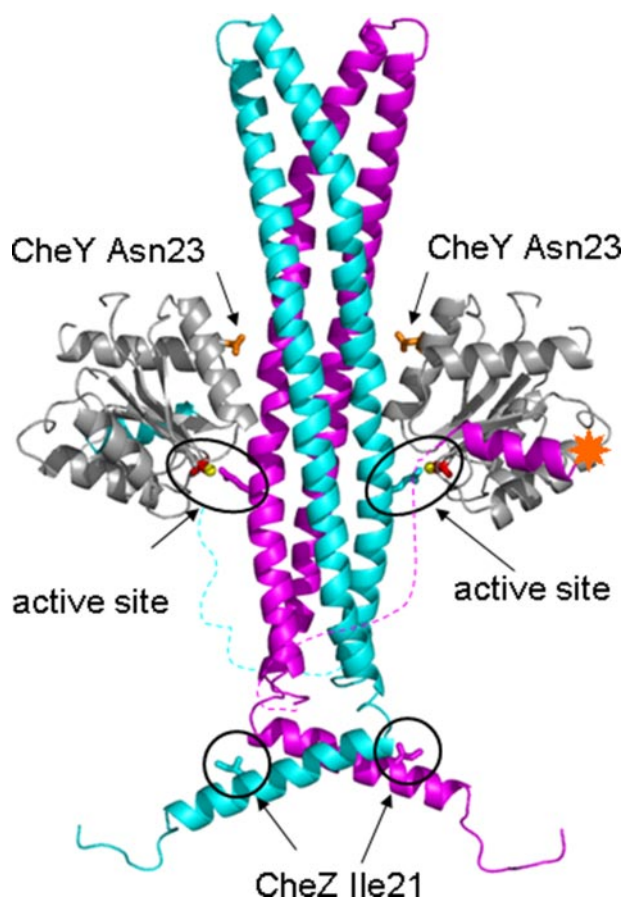


FIGURE 1. The CheZ_2 ($\text{CheY} \cdot \text{BeF}_3^- \cdot \text{Mg}^{2+}$) $_2$ ribbon structure (Protein Data Bank 1KMI) (18) with features pertinent to this study marked. The two identical chains comprising CheZ_2 are in magenta and cyan, and CheY is in gray. The ovals encase the two identical CheZ active site regions with essential catalytic residue Gln-147 of each CheZ monomer shown in stick form in the color of its parent chain, BeF_3^- in red and Mg^{2+} in yellow. The bottom circles encase CheZ Ile-21 in the color of the parent chain, and CheY Asn-23 is orange. The orange star marks the location of the badan fluorophore (CheZ C-terminal residue 214); an identical site located on the CheZ C terminus of the other CheZ chain (cyan) is not visible in this view of the complex. The 32-residue disordered linkers that were not visible in the crystal structure are sketched in as dotted lines. Because the co-crystal structure did not reveal the connectivity between the C-helix and the rest of the CheZ monomer, the designation of either C-helix as cyan or magenta is not certain.

CheY binds to the hydrophobic face of the CheZ C-helix. In the other interaction the active site region on CheY interacts with a surface near the center of the four-helix bundle of CheZ. Within the latter interaction surface, the essential catalytic residue Gln-147 from CheZ inserts into the CheY active site and is positioned to interact with a water molecule for in-line nucleophilic attack of the phosphoryl group, the same mechanism that has been proposed for CheY autodephosphorylation (21).

Although the catalytic roles of the CheZ C-helix and the central region of the four-helix bundle have been elucidated, the function of the N-terminal helices and the non-hairpin region of the bundle is still not understood. However, there is some evidence that this region may be involved in regulation of CheZ activity. Many of the CheZ mutants that display a “gain of function” phenotype (Che⁻, CCW flagellar rotation) (9, 11) map to this region of CheZ, which is distal from the characterized catalytic surfaces. Several of the gain of function mutants display

modest (2–5×) enhancements of CheZ activity when tested in a gel-based assay monitoring the loss of radioactivity from [³²P]CheYp (9, 11). Analysis of presteady state time courses that monitor the CheZ-induced shift in the equilibrium between CheYp and CheY suggested that CheZ catalytic activity exhibits positive cooperativity with respect to CheYp concentration. In contrast, the gain of function mutant CheZ-R54C displays enhanced phosphatase activity at low CheYp concentrations, suggesting that the substitution resulted in a constitutively activated state (22). These observations suggest CheZ activity might be regulated in a manner that could potentially play an important role in control of CheYp levels in the cell.

Here, we further explore the fundamental kinetic properties of catalysis by CheZ to acquire a more quantitative understanding of CheZ activity and possible regulation. With a standard enzymological approach, we measured CheZ catalytic activity at steady state as a function of substrate (CheYp) concentration to assess the presence of regulation by CheYp and determine kinetic constants. To complement the enzymology, we characterized the kinetics of association and dissociation of the CheZ-CheYp complex using CheYp-dependent fluorescence changes in CheZ covalently labeled with the badan fluorophore. Results from measurements made on both wild type CheZ and the gain of function mutant CheZ-I21T were combined to formulate a kinetic model for CheZ-mediated dephosphorylation that includes positive cooperativity with respect to CheYp. The model was used in computer simulations to predict CheZ activities at concentrations of CheZ and CheYp present in the cell.

EXPERIMENTAL PROCEDURES

Site-directed Mutagenesis and Protein Purification—The mutants *cheZ*-I21T and *cheZ*-I21T/F214C were constructed using the QuikChange mutagenesis kit (Stratagene) by introduction of the codon for Thr-21 into a pRS3 plasmid encoding either wild type CheZ or CheZ-F214C (8). Purification of CheZ (wild type and CheZ-I21T, -F214C, or -I21T/F214C) was carried out according to published procedures (23) with 2 mM dithiothreitol present during purification of CheZ proteins containing the cysteine substitution at position 214. Unlike wild type CheZ and CheZ-I21T, both CheZ-F214C and CheZ-I21T/F214C exhibited detectable proteolysis of the C-terminal 42 residues (8) after the standard purification procedure. These proteins were, therefore, subjected to an additional high resolution ion exchange step (Mono Q, GE Biosciences), which separated full-length from proteolyzed CheZ₂ (24). CheY (wild type, N23D, N59R, and A113P) was purified according to published procedures (25).

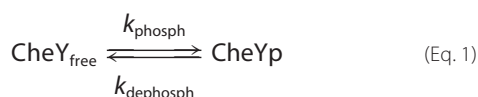
Kinetics of CheZ-catalyzed Dephosphorylation of CheY—The rate of dephosphorylation of CheY in the presence or absence of CheZ was measured using the EnzChek P_i assay (Invitrogen) adapted to a 96-well plate format from a previously described cuvette based assay (23). Wild type CheY was mixed with wild type CheZ (0, 50 nM, or 3.0 μM) in a total volume of 46 μl in buffer containing 50 mM Hepes, pH 7.0, 10 mM MgCl₂, and 1 mg/ml bovine serum albumin in a flat-bottomed polyethylene 96-well plate. At 30-s intervals, 4 μl of 50 mM monophosphimidazole (MPI; synthesized according to Rathlev and Rosenberg (26)) was added and mixed by repetitive pipetting to give a

Kinetics of CheZ Phosphatase

final concentration of 4 mM MPI. After the designated reaction time (22–30 min at room temperature), the reactions were quenched with 150 μ l of a solution containing 250 mM Tris, pH 7.5, 25 mM EDTA, 310 μ M 2-amino-6-mercapto-7-methylpurine riboside and 1.4 units/ml purine nucleoside phosphorylase. The high EDTA concentration stops both phosphorylation and dephosphorylation reactions, and the assay kit components 2-amino-6-mercapto-7-methylpurine riboside and purine nucleoside phosphorylase convert the P_i into a product with a detectable absorbance. After 15 min of incubation, the absorbances at 360 nm were read with a plate reader (Molecular Devices SpectraMax M2^e). The absorbance values were converted into P_i release rates (μ M P_i /s) using an empirically determined extinction coefficient derived from a standard P_i curve. All rates were corrected for the small amount of background P_i (introduced from the MPI preparations) deduced from controls lacking CheY. Preliminary experiments demonstrated that the rates were linear for at least 1 h. For experiments comparing the activities of wild type CheZ and CheZ-I21T, CheY-A113P was used as the substrate due to its enhanced autophosphorylation rate (27). This was manifested in higher rates of P_i release in the presence of excess CheZ, which allowed a larger range of dephosphorylation rate measurements at low CheYp concentrations.

For a subset of the enzyme kinetic experiments, duplicates of each reaction condition were included, and the absorbance values were averaged. In these cases the duplicates were in excellent agreement, and use of the averaged values did not significantly affect the curve fit to the data relative to using single readings. Therefore, for most of the experiments, single reactions of each CheZ/CheY concentration condition were used to limit the number of samples so that the reactions could be quenched within 30 min. The results of multiple (three or four) independent experiments for each CheZ and CheY combination were averaged to get the final kinetic values. To measure time courses, reactions were scaled up in volume keeping all components at the same concentrations used in the single time point analysis. After initiation of the reaction by the addition of monophosphoimidazole, 50- μ l aliquots were removed at various times, placed in a new well of the microtiter plate, and assayed for P_i as described above.

For analysis of the dephosphorylation rate data, consideration was made of the following equilibrium,



where k_{phosph} is the pseudo-first order rate constant for phosphorylation at 4 mM MPI, and k_{dephosph} is the first order rate constant for dephosphorylation. First, k_{phosph} was determined using the slope of the linear relationship between the rate of P_i release and CheY concentration in the presence of excess CheZ (3 μ M). Under these conditions, dephosphorylation occurs rapidly, so that CheY is mostly unphosphorylated ($\text{CheY}_{\text{free}}$), and the measured rate of P_i release = $k_{\text{phosph}}(\text{CheY}_{\text{total}})$ (*i.e.* phosphorylation is rate-limiting). Next, the concentration of CheYp present at steady state for each sample was calculated using the

following relationships derived from Equation 1.

$$[\text{CheY}_{\text{free}}] \times k_{\text{phosph}} = [\text{CheYp}] \times k_{\text{dephosph}} = \text{rate of } P_i \text{ release} \quad (\text{Eq. 2})$$

Solving for $[\text{CheY}_{\text{free}}]$,

$$[\text{CheY}_{\text{free}}] = \text{rate of } P_i \text{ release} / k_{\text{phosph}} \quad (\text{Eq. 3})$$

and

$$[\text{CheYp}] = [\text{CheY}_{\text{total}}] - [\text{CheY}_{\text{free}}]. \quad (\text{Eq. 4})$$

Finally, the rate of P_i release due only to CheZ was determined for each data point by subtracting the amount of P_i release expected in the absence of CheZ (derived from the linear relationship between P_i release and CheYp concentration in the absence of CheZ) from the P_i release rate in the presence of CheZ.

The data were fit using nonlinear regression (Prism software) directly to the Hill equation

$$v = V_{\text{max}}[\text{CheYp}]^n / (K_{0.5}^n + [\text{CheYp}]^n) \quad (\text{Eq. 5})$$

with V_{max} , $K_{0.5}$ (the concentration of CheYp necessary for half-maximal velocity), and n (the Hill coefficient) as floating variables.

Labeling CheZ with the Badan Fluorophore—Fractions from the Mono Q salt gradient elution that contained only full-length CheZ-F214C or CheZ-I21T/F214C were pooled and immediately supplemented with 1 mM tris-2-carboxyethyl phosphine hydrochloride (Pierce) to keep Cys-214 reduced. The badan (6-bromoacetyl-2-dimethylaminonaphthalene; Invitrogen) was prepared fresh as a 25 mM stock solution in dimethylformamide. The badan solution was added to the CheZ (100 μ M) in 5 equal aliquots at 5-min intervals while stirring to give a final concentration of 1 mM badan. The reaction was placed in the dark for 2 h at room temperature, quenched by the addition of 10 mM dithiothreitol, and clarified by centrifugation to remove a small amount of insoluble matter generated during the reaction. The clarified sample was then chromatographed on G-75 Sephadex in 50 mM Tris, pH 7.5, 0.5 mM EDTA, 10% (v/v) glycerol, 2 mM dithiothreitol to separate the badan-labeled CheZ from unreacted badan. The protein concentration of badan-labeled CheZ (*B-CheZ or *B-CheZ-I21T) was determined using a Bradford assay (Bio-Rad protein assay kit) with unlabeled CheZ as a standard. The concentration of badan in the labeled protein was determined by the absorbance at 392 nm ($\epsilon = 12.9 \text{ mM}^{-1} \text{ cm}^{-1}$) (28). Labeling ratios were 1.2 and 0.7 mol/mol for *B-CheZ and *B-CheZ-I21T, respectively.

Fluorescence Measurements—Steady state fluorescence measurements of *B-CheZ or *B-CheZ-I21T were made on a PerkinElmer Life Sciences LS-50B spectrofluorimeter with a circulating water bath to maintain cuvette temperature at 20 °C. For emission scans, the excitation wavelength was 392 nm, and the emission was scanned from 400 to 600 nm. For time courses and equilibrium titrations, the excitation wavelength was 392 nm, and the emission wavelength was 500 nm for *B-CheZ and 470 nm for *B-CheZ-I21T. Excitation and emission slit widths were adjusted to optimize the signal/noise

ratio. For equilibrium titration of *B-CheZ or *B-CheZ-I21T with CheYBeF₃ or CheY-N23DBeF₃, badan-CheZ was diluted to 0.1 μM in buffer containing 50 mM Hepes, pH 7.0, 10 mM MgCl₂, 10 mM NaF, and 0.1 mM BeCl₂. Repetitive additions of small volumes of CheY were made, and the fluorescence was monitored continuously. Subsequent additions were made only after the fluorescence had stabilized as a result of the previous addition. The final intensities were corrected for the dilution due to the addition of CheY. For measurement of emission spectra and equilibrium titrations, a 1 × 1-cm cuvette was used (sample volume, 1.5 ml) with magnetic stirring. The cuvette chamber was left open during experiments to eliminate the sensitivity of the fluorescence signal to opening and closing of the cuvette chamber.

*B-CheZ·CheYBeF₃ dissociation time courses were monitored at 20 °C using a rapid mixing accessory (Applied Photophysics RX-2000) in conjunction with the PerkinElmer LS-50B spectrofluorimeter. In these experiments, one syringe of the rapid mixer contained *B-CheZ (1.0 μM) and CheY (2.0 μM) in buffer containing 50 mM Hepes, pH 7.0, 10 mM MgCl₂, 0.10 mM BeCl₂, and 10 mM NaF. The other syringe contained unlabeled CheZ (20 μM; either wild type or CheZ-I21T to match the CheZ used in the complex) in the same buffer. Mixture of the two solutions resulted in recovery of the fluorescence of uncomplexed *B-CheZ at a rate that reflects dissociation of CheYBeF₃ from the badan-CheZ·CheYBeF₃ complex. For each CheZ 6–8 repetitive time courses were recorded with data points taken every 100 ms. Data from each time course were fit to an equation describing a single exponential decay using nonlinear regression (Prism), and the first order rate constants of the repetitive shots were averaged. The resultant rate constants from two to three independent experiments for both wild type CheZ and CheZ-I21T were then averaged.

To measure the kinetics of association of *B-CheZ or *B-CheZ-I21T with phosphorylated CheY-N59R, a SPEX Fluorolog-3 spectrofluorimeter equipped with a Jobin Yvon Horiba F-3009 Microflow stop flow device (dead time, ~5 ms) was used. For these experiments, one syringe contained 0.4 μM badan-CheZ (*B-CheZ or *B-CheZ-I21T) in reaction buffer (50 mM Hepes, pH 7.0, 10 mM MgCl₂), and the other syringe contained CheY N59R (2–60 μM) in reaction buffer supplemented with 20 mM phosphoramidate (synthesized according to Sheridan *et al.* (29)). The experiments were carried out at room temperature (22–23 °C) or at a constant temperature of 23 °C using a circulating thermostatted water bath. For each CheY concentration, 4–13 time courses were recorded by repetitive shots, and data were recorded at 10-ms intervals for *B-CheZ reactions and 2-ms intervals for *B-CheZ-I21T reactions. The data (the first 300 ms for *B-CheZ and 60 ms for *B-CheZ-I21T) were fit to a single exponential decay using nonlinear regression (Prism). CheY-N59Rp binds efficiently to CheZ but is resistant to its phosphatase activity (23) and was used in these experiments to avoid the toxicity of beryllium.

Computer Simulations—Rate equations for the reaction scheme presented under “Discussion” were derived and encoded in a C++ program employing Euler’s method as the numerical integrator. Each simulation was run for 60 s of simulated time to reach steady state. Inputs to the program are the

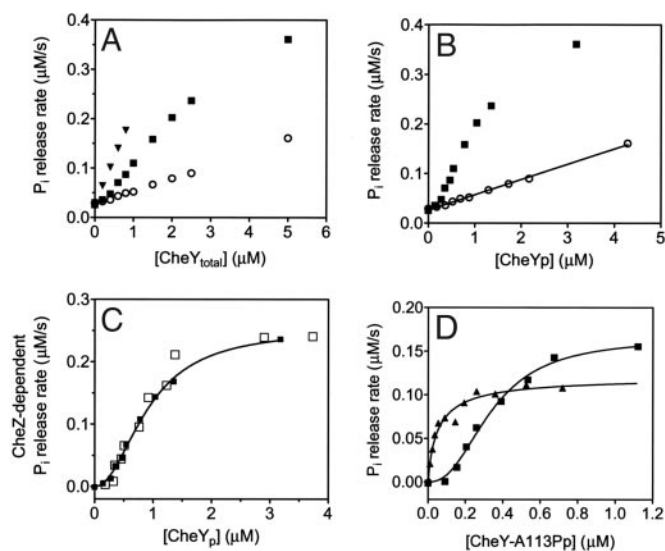


FIGURE 2. Steady state dephosphorylation kinetics of CheZ. A, representative raw data with absorbances at 360 nm converted to P_i release rates for reactions carried out in the absence of CheZ (open circles), in the presence of 50 nM CheZ (closed squares), or 3 μM CheZ (closed triangles). B, the data in panel A were corrected for the concentration of CheYp present at steady state under each reaction condition and replotted. Reactions carried out in the absence of CheZ (open circles) or presence of 50 nM CheZ (closed squares). The line represents the best fit to the rates in the absence of CheZ. C, final analysis represents the subtraction of the P_i release expected in the absence of CheZ (determined from the equation of the line shown in panel B) from each rate measured in the presence of 50 nM CheZ. The results are shown for two independent trials. Trial 1 (closed squares) is the data shown in panels A and B. Trial 2 (open squares) is data from an independent experiment. The curve shown is the best fit to the Hill equation for Trial 1 using nonlinear regression. Note different x axis scales in panels A–C. D, final data analysis for representative experiment measuring P_i release kinetics of 50 nM wild type CheZ (closed squares) or 50 nM CheZ-I21T (closed triangles) with CheY-A113Pp as substrate. The curves represent the best fit to the Hill equation using nonlinear regression.

amounts of unphosphorylated CheY and CheZ and a set of rate constants for the reactions; outputs of the program are the concentration of CheYp and the rate of phosphate release at time 60 s, given an external source of phosphoryl groups in excess. The simulations were performed on a PowerPC G4 running Mac OS X Version 10.4.9.

RESULTS

Steady State Kinetic Analysis of Dephosphorylation of CheYp Mediated by Wild Type CheZ Indicates Positive Cooperativity—The rate of P_i release in reactions containing various amounts of CheY (0 to 5 μM), 4 mM monophosphoimidazole, and either 0, 50 nM, or 3 μM CheZ were measured and plotted as a function of total CheY concentration (Fig. 2A). Rates of P_i release in the absence of CheZ reflect CheY autodephosphorylation, and rates in the presence of 3 μM (excess) CheZ represent the fastest rate of P_i release possible at each CheY concentration, *i.e.* the rate of CheY autophosphorylation. Analysis of the raw data as described under “Experimental Procedures” first involved calculation of the concentration of CheYp present under each steady state reaction condition (Fig. 2B), which finally led to the relationship between CheZ activity and CheYp concentration (Fig. 2C). This relationship displayed marked sigmoidicity, suggesting the presence of positive cooperativity. Fitting the data from three independent experiments

Kinetics of CheZ Phosphatase

to the Hill equation gave a Hill coefficient of 2.1 ± 0.3 (see Fig. 2C for sample curve fit), a $K_{0.5}$ value of $0.8 \pm 0.1 \mu\text{M}$, and a k_{cat} of $4.9 \pm 0.1 \text{ s}^{-1}$. Several control experiments were performed to ensure that the rates measured at low CheYp were not an artifact of the experimental process due to the small magnitudes of P_i release rates in the presence and absence of CheZ. First, time courses of P_i release were carried out for reactions containing 0.2, 0.4, and 0.6 μM CheY ($\pm 50 \text{ nM}$ CheZ) for 80 min rather than the standard 30 min. The rates were linear over the entire time course, eliminating the possibility that a lag phase contributed to low activity. Furthermore, the longer time points (with larger differences in absorbance in the presence and absence of CheZ) gave the same specific activity as those measured in the single time point experiment, thus excluding low absorbances as a source of error. Second, the concentration of bovine serum albumin in the reaction buffer was varied between 0, 0.10, 0.50, and 1 mg/ml with no change in results, implying that the low concentrations of CheY present in these reactions were not adsorbed on to the surface of the microtiter plate.

Comparative Kinetic Analysis for Gain of Function Mutant CheZ-I21T Indicates Loss of Cooperativity—Cells containing CheZ-I21T are incapable of chemotaxis due to constitutively counterclockwise flagellar rotation, consistent with an increase in CheZ phosphatase activity (30). Ile-21 is located on the N-helix, close to the bottom of the four helix bundle and more than 40 Å from the active site (Fig. 1). Preliminary experiments for kinetic analysis of CheZ-I21T showed that at 50 nM CheZ-I21T (the same concentration of CheZ used in the wild type CheZ experiment), the rate of P_i release at low CheY concentrations (0.1–0.4 μM) was the same as that for 3 μM (excess) CheZ, whereas V_{max} was approximately unchanged (data not shown). Therefore, at low CheY concentrations, CheZ-I21T was dephosphorylating CheY as fast as it was being phosphorylated, precluding determination of accurate rates. Therefore, for analysis of CheZ-I21T, we used the CheY-A113P mutant whose autophosphorylation is 6-fold faster but has similar CheZ sensitivity as wild type CheY (27). These features should give higher rates of P_i release in the presence of excess CheZ and, therefore, a larger window in which to assess activity due to limiting amounts of CheZ. As predicted, the data demonstrated a slope for P_i release rate from CheY-A113P in the presence of excess CheZ that was about 3.5 times the slope for wild type CheY (data not shown). Final analysis of the data using catalytic (50 nM) wild type CheZ revealed sigmoidicity with respect to CheY-A113Pp (Fig. 2D) as observed with wild type CheYp, with only modest changes in other kinetic parameters. Kinetic parameters derived from three independent measurements gave a Hill coefficient of 2.2 ± 0.2 , $K_{0.5}$ of $0.3 \pm 0.1 \mu\text{M}$, and k_{cat} of $3.5 \pm 0.3 \text{ s}^{-1}$. In contrast, CheZ-I21T displayed apparently hyperbolic kinetics with enhanced activity relative to wild type CheZ at low CheY concentrations but had a similar k_{cat} as wild type CheZ (Fig. 2D). The kinetic parameters for CheZ-I21T averaged from three independent experiments gave a Hill coefficient of 1.2 ± 0.3 , $K_{0.5}$ of $0.08 \pm 0.03 \mu\text{M}$, and a k_{cat} of $2.7 \pm 0.3 \text{ s}^{-1}$. Therefore, a predominant effect of the CheZ-I21T substitution is to eliminate the positive cooperativity observed with wild type CheZ while enhancing activity at low CheYp concen-

trations. This suggests that the positive cooperativity displayed by wild type CheZ depends on structural features present at the nonhairpin end of the four-helix bundle (Fig. 1).

Monitoring CheZ-CheY Complex Formation Using Badan-CheZ—Previous studies exploited two CheY derivatives to monitor the interaction of CheZ and CheYp without the complication of catalytic removal of the phosphoryl group. CheY-N59Rp binds to CheZ but is resistant to its phosphatase activity due to a salt bridge between CheY Arg-59 and CheY Glu-89, which is essential for CheZ activity (23, 31). CheYBeF₃ is a stable derivative of CheYp that has proven to be an excellent structural and functional analogue of CheYp (18, 19). CheZ binds both CheY N59Rp and CheYBeF₃ with sufficiently high affinity that there is essentially quantitative complex formation when both proteins are present at 200 nM, indicating a submicromolar K_d value (23).

To further probe the interaction between CheZ and CheYp for the purposes of evaluating how this high affinity affects the overall kinetic mechanism of CheZ catalysis, we sought a method to directly monitor time courses for both association and dissociation of the CheZ-CheYp complex. Badan is a fluorophore whose emission is highly sensitive to its local environment and was, thus, a candidate for use as a probe to monitor the CheZ/CheYp interaction. Position 214 of CheZ (phenylalanine in wild type CheZ) is the C-terminal residue of the C-helix and is adjacent to the $\alpha_4\beta_5\alpha_5$ binding surface of CheYBeF₃ in the CheZ-CheYBeF₃ structure (Fig. 1) (18, 32). The emission spectra of both *B-CheZ and *B-CheZ-I21T ($\lambda_{\text{ex}} = 392 \text{ nm}$) underwent substantial degrees of quench (~ 40 –50% of maximal intensity) upon binding CheYBeF₃ (Fig. 3A), indicating that these labeled CheZs could serve as useful probes for monitoring CheZ/CheYp binding events. However, although the fluorescence emission spectra of the complexed *B-CheZ and *B-CheZ-I21T were very similar, there was a substantial difference in the emission spectra of the derivatized CheZs in their uncomplexed forms. The emission spectrum of *B-CheZ ($\lambda_{\text{max}} = 500 \text{ nm}$) was red-shifted more than 30 nm relative to *B-CheZ-I21T ($\lambda_{\text{max}} = 470 \text{ nm}$). This suggests that the fluorophores, located on the C-helix of CheZ, experience different environments in the wild type *versus* the gain of function CheZ-I21T. Emission spectra of *B-CheZ complexed to CheY N59Rp or wild type CheYp (using phosphoramidate as a phosphodonor) were very similar to the CheZ-CheYBeF₃ spectrum (data not shown). Control experiments that varied the order of addition of components demonstrated that the emission spectrum characteristic of complex formation (Fig. 3A) depended on the presence of all components: CheZ, CheY, Mg^{2+} , and either BeF_3^- or phosphoramidate. *B-CheZ displayed catalytic properties similar to wild type CheZ (Fig. 2) when its activity was measured as a function of wild type CheYp (data not shown). The relationship was sigmoidal with $K_{0.5} \sim 1.4 \mu\text{M}$ and $k_{\text{cat}} \sim 3 \text{ s}^{-1}$ (cf. Fig. 2C).

Equilibrium titrations of the fluorescence of *B-CheZ with CheYBeF₃ (Fig. 3B) demonstrated the expected high affinity concluded from other studies. At 0.1 μM *B-CheZ, approximately equimolar amounts of CheYBeF₃ were required to saturate the change in fluorescence, indicating that nearly all of the

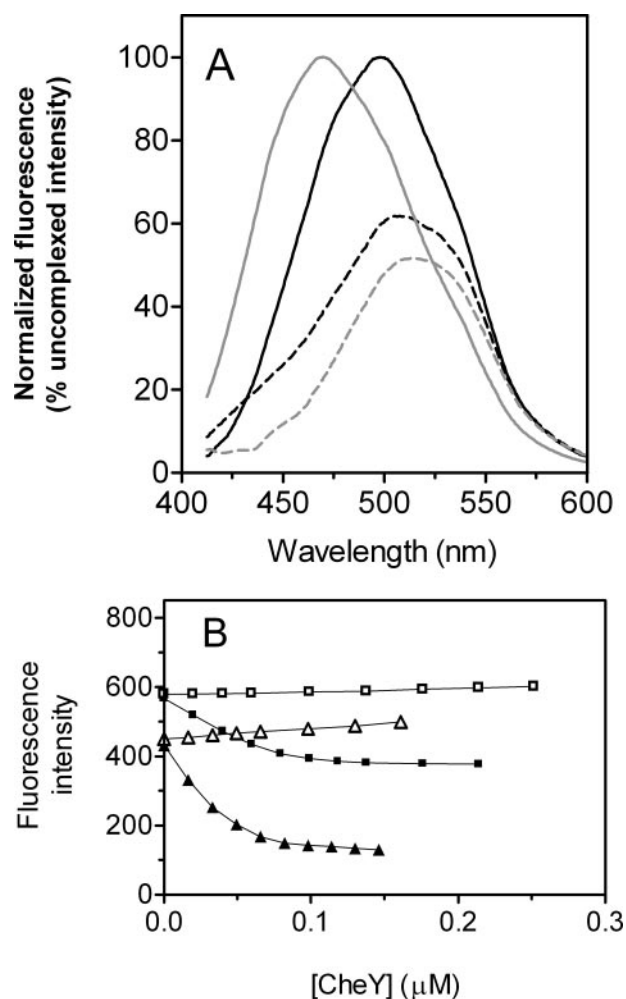


FIGURE 3. Sensitivity of the fluorescence intensity of the badan fluorophore attached to the C terminus of CheZ to complex formation with CheYBeF₃. A, fluorescence emission spectra of badan-labeled CheZ in the presence and absence of CheYBeF₃. The excitation wavelength was 392 nm. Solid black line, *B-CheZ; dashed black line, *B-CheZ-CheYBeF₃; solid gray line, *B-CheZ-I21T; dashed gray line, *B-CheZ-I21T-CheYBeF₃. Spectra of uncomplexed *B-CheZ and *B-CheZ-I21T were normalized independently to 100%, and spectra of their respective complexed forms were plotted relative to the uncomplexed form of the same CheZ. B, equilibrium titration of the fluorescence intensity of 0.1 μM badan-CheZ with CheY. Shown are *B-CheZ titrated with CheY in the presence (closed squares) and absence (open squares) of BeF₃ and *B-CheZ-I21T titrated with CheY in the presence (closed triangles) and absence (open triangles) of BeF₃.

added protein was bound. A similar titration using *B-CheZ-I21T also displayed essentially quantitative binding (Fig. 3B). Similar fluorescence results were obtained when badan was covalently attached to Cys-210 in the CheZ derivative 210DC indicating that neither the phenylalanine to cysteine substitution nor the badan derivatization at position 214 specifically disrupted an essential CheZ/CheYp interaction.

Association Kinetics of B-CheZ and CheYp—Time courses monitoring the association of *B-CheZ or *B-CheZ-I21T with CheY N59Rp were recorded under pseudo-first order kinetic conditions using stopped flow fluorescence spectroscopy. For both CheZs, the time courses fit well (average $R^2 = 0.98$ for *B-CheZ and 0.96 for *B-CheZ-I21T) to equations describing a single exponential decay (see Fig. 4A for sample time courses and curve fits). Plots of the pseudo-first order rate constants

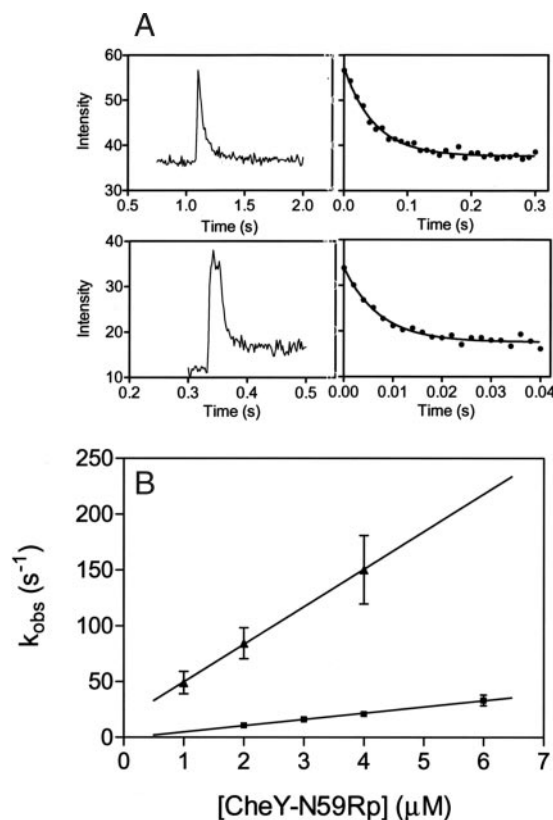


FIGURE 4. Association kinetics of badan-CheZ and CheY N59Rp measured by stopped flow fluorescence. A, representative time courses (left) and curve fits (right) for association of *B-CheZ (top) and *B-CheZ-I21T (bottom) with CheY N59Rp. Note the different time scales. The concentrations of CheZ and CheY N59Rp were 0.2 and 4 μM, respectively. B, representative plots of k_{obs} versus the CheY N59Rp concentration for *B-CheZ (closed squares) and *B-CheZ-I21T (closed triangles). The lines represent linear regression fits of the data, and the slopes are equal to the bimolecular rate constants for association (k_{assoc}). Error bars represent the S.D. from the mean of multiple sequential reaction time courses ($n = 4-11$) and are smaller than the size of the data point when not visible.

(k_{obs}) versus CheY-N59Rp concentration were linear (Fig. 4B), indicating a rate-limiting step that was a bimolecular process. The slopes of the lines gave the bimolecular rate constants. The value for *B-CheZ ($5.64 \pm 0.02 \times 10^6 \text{ M}^{-1} \text{ s}^{-1}$; average and S.D. of two independent measurements) is well within the window typically observed for protein/protein association events (33). Strikingly, the k_{assoc} value for *B-CheZ-I21T was 6-fold faster ($3.36 \pm 0.01 \times 10^7 \text{ M}^{-1} \text{ s}^{-1}$). This enhanced k_{assoc} value likely contributes to the shift of the kinetic profile of CheZ-I21T to lower CheYp concentrations relative to wild type CheZ (Fig. 2D) and may also explain the loss of cooperativity (see “Discussion”). The observation that the pseudo-first order rate constant was proportional to CheYp concentration indicated that the rate-limiting step in association of wild type CheZ and CheZ-I21T with CheYp is the association of the first binding surface; association of the second surface must ensue rapidly. This experiment does not distinguish the order of binding events for CheYp to the two binding surfaces of CheZ.

Dissociation Kinetics of the CheZ-CheYBeF₃ Complex—While continuously monitoring fluorescence, the addition of 0.1 μM CheYBeF₃ to 0.1 μM *B-CheZ or 0.1 μM *B-CheZ-I21T resulted in a time-dependent quench due to formation of the

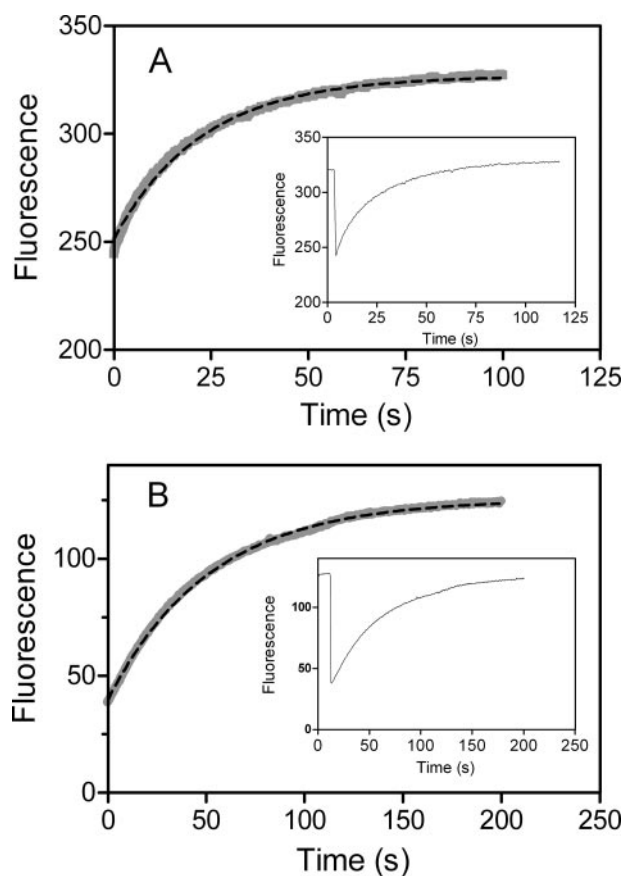


FIGURE 5. Kinetics of dissociation of the badan-CheZ-CheYBeF₃ complex. Representative fluorescence time courses reflecting dissociation of *B-CheZ-CheYBeF₃ (A) and *B-CheZ-I21T-CheYBeF₃ (B) (note different time scales). For both panels, the data points are in gray, and the curve fit for a single exponential process is shown as a dashed line. The insets are traces of the raw fluorescence data.

CheZ-CheYBeF₃ complex. After the change in fluorescence had stabilized, the addition of a 20-fold excess of unlabeled CheZ resulted in a time-dependent increase in fluorescence until the initial fluorescence had been recovered (data not shown). Under these conditions, the CheYBeF₃ that dissociates from the complex will nearly always reassociate with unlabeled CheZ so that the rate of recovery of the fluorescence of unbound *B-CheZ reflects the rate of dissociation of the CheZ-CheYBeF₃ complex. To rigorously measure the rate of dissociation, the CheZ-CheYBeF₃ complex was mixed with excess CheZ using a rapid mixing apparatus, and the time courses were recorded. The time courses for dissociation fit well to single exponential decays ($R^2 > 0.99$, Fig. 5), and the deduced k_{dissoc} values from 5–6 successive shots through the apparatus were averaged for each experiment. The k_{dissoc} values (average of two or three independent experiments) were $0.040 \pm 0.004 \text{ s}^{-1}$ for the wild type CheZ-CheYBeF₃ complex and $0.023 \pm 0.001 \text{ s}^{-1}$ for the CheZ-I21T-CheYBeF₃ complex. Taking the measured k_{assoc} and k_{dissoc} values for calculation of $K_d = k_{\text{dissoc}}/k_{\text{assoc}}$ gives K_d values of 7.1 and 0.68 nM for binding of CheYBeF₃ to wild type CheZ and CheZ-I21T, respectively. The analogous experiment using CheY-N59Rp and *B-CheZ gave a dissociation rate constant of 0.13 s^{-1} (data not shown). The increase in rate relative to the CheYBeF₃ experiment likely reflects the fact that autode-

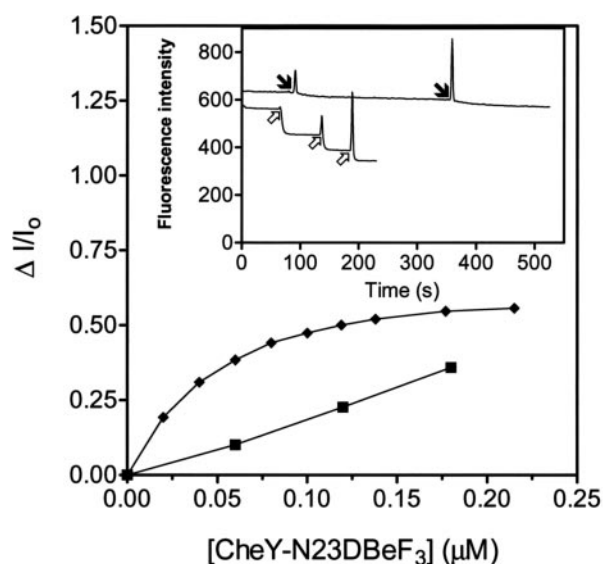


FIGURE 6. Equilibrium titrations of *B-CheZ and *B-CheZ-I21T with CheY-N23DBeF₃. Fluorescence changes upon the addition of incremental amounts of CheY-N23DBeF₃ to $0.1 \mu\text{M}$ *B-CheZ (squares) or *B-CheZ-I21T (diamonds) measured at equilibrium. The inset shows the raw data for the first several additions. Top, *B-CheZ with additions of $0.060 \mu\text{M}$ CheY-N23DBeF₃ at the times designated with a solid arrow. Bottom, *B-CheZ-I21T with additions of $0.020 \mu\text{M}$ CheY-N23DBeF₃ at times designated with an open arrow.

phosphorylation ($k \sim 0.04 \text{ s}^{-1}$) (34) and/or modest CheZ-mediated dephosphorylation is likely followed by rapid dissociation of the CheZ-CheY-N59Rp complex.

*Equilibrium Binding of *B-CheZ and *B-CheZ-I21T to CheY-N23D*—CheY Asn-23 is located on the $\alpha 1$ helix and interacts with the CheZ four-helix bundle. Accordingly, CheY-N23D is partially resistant to CheZ phosphatase activity due to diminished binding to CheZ (35). Interestingly, when CheZ phenotypic suppressors of CheY-N23D were originally isolated, many were also gain of function mutants, *i.e.* they conferred a Che⁻ phenotype due to counterclockwise flagellar rotation for strains containing wild type CheY. CheZ-I21T was isolated independently from screens for gain of function mutants (9) and for CheY-N23D suppressors (30). We measured equilibrium binding of CheYBeF₃ or CheY-N23DBeF₃ to *B-CheZ or *B-CheZ-I21T (Fig. 6). At $0.1 \mu\text{M}$ *B-CheZ, the addition of substoichiometric quantities of CheY-N23DBeF₃ resulted in modest fluorescence changes. In contrast, the response of *B-CheZ-I21T to the same titration was of greater magnitude (Fig. 6, inset). Plotting the degree of fluorescence changes as a function of CheY-N23DBeF₃ concentration showed that for *B-CheZ, the binding was decreased from the quantitative binding of wild type CheYBeF₃ under the same conditions. However, for CheZ-I21T the binding was essentially quantitative. Therefore, CheZ-I21T compensates for the defective binding of CheY-N23D, presumably through the enhanced association rate demonstrated above. This result provides an explanation for why the same CheZ mutants were identified in both genetic screens.

DISCUSSION

Fundamental Enzymatic Properties of the CheZ Phosphatase—Here we determined several fundamental kinetic parameters

that describe CheZ-catalyzed dephosphorylation of its physiological substrate, CheYp. Measurement of enzyme activity as a function of substrate concentration revealed strong positive cooperativity with respect to CheYp. Independent measurement of the association and dissociation rates of CheZ and CheYp implicated a dissociation constant of 7.1 nM, markedly lower than intracellular concentrations of either protein (36). However, because k_{dissoc} (0.040 s^{-1}) \ll k_{cat} (4.9 s^{-1}), CheZ and CheYp are not expected to be in binding equilibrium during catalysis, and nearly every binding event will result in dephosphorylation of CheY.

Regulation of CheZ Activity by CheYp; Positive Cooperativity—The observation here of sigmoidicity, an indicator of positive cooperativity, in the relationship between steady state CheZ activity and CheYp concentration is in agreement with an earlier study that used a pre-steady state kinetic approach (22). This finding implicates a mechanism by which the cell could temper CheZ phosphatase activity when intracellular CheYp concentrations are low or, conversely, maximize activity when CheYp levels are high. Computer simulations have predicted that such CheYp-induced activation of CheZ would increase the robustness of the chemotaxis system toward cell-to-cell variation in chemotaxis proteins (37, 38) and implicate a role for CheZ in adaptation, the ability of the cell to return CheYp levels toward pre-stimulus levels after the stimulus is removed (39).

Here, we further demonstrated that the kinetics of the gain of function mutant CheZ-I21T did not display positive cooperativity and had markedly enhanced phosphatase activity but only at low CheYp concentrations (subsaturating for wild type CheZ). Cells containing CheZ-I21T cannot mediate chemotaxis because of constitutively counterclockwise flagellar rotation and consequent inability to tumble (30), a result of low CheYp. Thus, it appears that for successful chemotaxis, there is an absolute requirement for reduction of CheZ phosphatase activity at low CheYp levels. The independent observation here that CheZ-I21T has an enhanced association rate with CheYp relative to wild type CheZ provides a plausible explanation for the higher activity at low CheYp. The faster association would result in higher occupancy of CheZ-I21T with CheYp relative to wild type CheZ when CheYp is limiting. Furthermore, the absence of positive cooperativity for CheZ-I21T implicates a role for the non-hairpin end of the CheZ four-helix bundle in regulation of CheZ catalytic activity.

Possible Kinetic Basis for Positive Cooperativity—Positive cooperativity is most often a result of communication between active sites within an oligomeric enzyme (40). The Hill coefficient of ~ 2 measured here is consistent with communication between the two active sites within the CheZ dimer. We used mathematical modeling to assess the compatibility of our kinetic data with a model whereby the second CheYp binds CheZ₂ with higher affinity than the first. The simulation included rate equations for each reaction in Scheme 1 and the simulation target was the uncorrected raw kinetic data (as in Fig. 2A) to avoid potential error introduced by estimation of CheYp concentrations. Starting with a model of noninteracting CheZ₂ active sites and using measured rate constants, the simulation predicted enzymatic activity for 50 nM CheZ that

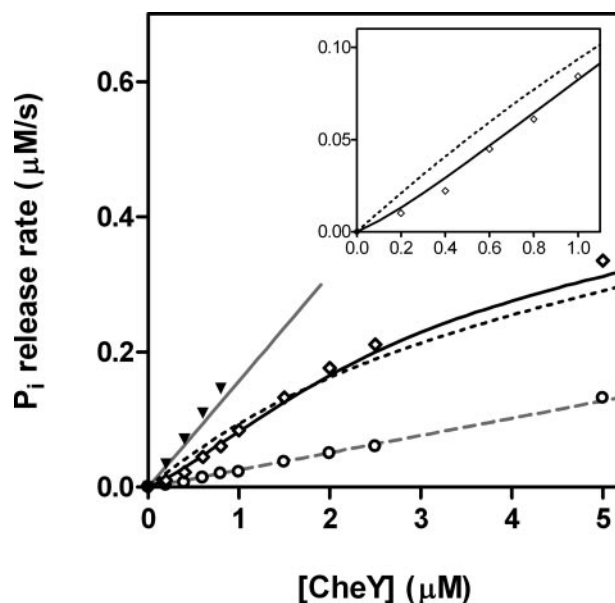
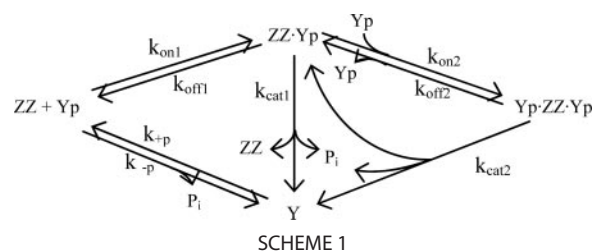


FIGURE 7. Simulations of CheZ-catalyzed dephosphorylation of CheY. The computer program described under “Experimental Procedures” was used to simulate the raw kinetic data in Fig. 2A. For each CheZ concentration, simulations were performed to determine the total (auto- and CheZ-catalyzed) phosphate release rate for initial CheY concentrations between 0 and 6 μM in increments of 0.1 μM . The experimental data are shown as symbols: closed triangles, excess CheZ; open diamonds, 50 nM CheZ; open circles, no CheZ. The simulation outputs are shown as lines: gray solid line, excess CheZ; gray dashed line, no CheZ; black dashed line, non-cooperative simulation for 50 nM CheZ with $k_{\text{on1}} = k_{\text{on2}} = 5.6 \times 10^6 \text{ M}^{-1} \text{ s}^{-1}$; black solid line, cooperative simulation for 50 nM CheZ with $k_{\text{on1}} = 9.2 \times 10^5 \text{ M}^{-1} \text{ s}^{-1}$ and $k_{\text{on2}} = 3.4 \times 10^7 \text{ M}^{-1} \text{ s}^{-1}$. For all simulations $k_{\text{cat1}} = k_{\text{cat2}} = 4.9 \text{ s}^{-1}$, $k_{\text{off1}} = k_{\text{off2}} = 0.040 \text{ s}^{-1}$, $k_{+p} = 0.17 \text{ s}^{-1}$, and $k_{-p} = 0.030 \text{ s}^{-1}$. Inset, expanded view of data for 50 nM CheZ at low CheY concentrations.

changed over a similar range of CheYp concentrations as measured experimentally (Fig. 7). However, as expected, this model did not predict sigmoidicity but, instead, predicted rates that were consistently higher than the experimental rates at low CheYp (Fig. 7, inset). The output of the simulation proved to be quite sensitive to modest changes in k_{on} (with the curves shifting to the lower CheYp as k_{on} increased) but was relatively insensitive to changes in k_{off} (data not shown). In contrast to the noninteracting site model, a reasonable fit to the experimental kinetic data was achieved with $k_{\text{on1}} < k_{\text{on2}}$ (Fig. 7). The k_{on1} and k_{on2} values used in the simulation (9.2×10^5 and $3.4 \times 10^7 \text{ M}^{-1} \text{ s}^{-1}$, respectively) (Fig. 7) are consistent with the measured wild type CheZ/CheYp association rate ($5.6 \times 10^6 \text{ M}^{-1} \text{ s}^{-1}$) because the measured rate reflects fluorescence quenching from association of both the first and second CheYp molecules and would be expected to be intermediate in magnitude between k_{on1} and k_{on2} . Furthermore, the measured k_{assoc} for CheZ-I21T, when used as a value for k_{on2} (Fig. 7), gave a reasonable fit to the experimental data, consistent with the possibility that the

Kinetics of CheZ Phosphatase

CheZ-I21T dimer may associate with both CheYp molecules at a similar rate as the second CheYp for wild type CheZ. A model with $k_{on1} < k_{on2}$ implies that k_{on1} is somehow suppressed for wild type CheZ. This suppression may be relieved by binding the first CheYp for wild type CheZ or by the CheZ-I21T mutant for binding both CheYp molecules.

The model described above accounts for the initially paradoxical observation of positive cooperativity for an enzyme that binds extremely tightly to its substrate. In this situation the occupancy of the enzyme with substrate is a function of k_{assoc} and k_{cat} (not K_m and k_{cat}) and, with the stipulation that $k_{on2} > k_{on1}$, predicts sigmoidicity in active site occupancy. However, we have not ruled out the possibility that the positive cooperativity observed for CheZ is due to a higher k_{cat} value (per site) when both active sites are occupied relative to when just one active site is occupied (40, 41).

Mechanism of CheZ/CheYp Association and Structural Basis for Enhanced k_{assoc} for CheZ-I21T—With two independent surfaces of interaction between CheZ and CheYp, association of the two proteins must occur in two sequential steps. Direct binding between CheYp and the isolated four-helix bundle was not detected in two independent studies (18, 42), whereas CheYp binds to the isolated C-helix with a K_d of 26 μM (43), making it probable that binding occurs first to the C-helix. The association kinetics between CheZ and CheYp demonstrated that the rate-limiting step for both wild type CheZ and CheZ-I21T involves the initial association with CheYp. The CheZ-I21T substitution may, therefore, affect the function of the linker/C-helix region with the result of enhancing the ability of the C-helix to bind CheYp. Ile-21 is proximal to the site where the linker emanates from the four-helix bundle (Fig. 1), so a substitution at that position could affect the position and/or motion of the linker, which has a high degree of mobility independent of the four-helix bundle when CheYp is not bound (24). The observation that the emission of the badan fluorophore linked to the C-helix of CheZ-I21T was blue-shifted 30 nm relative to wild type CheZ (Fig. 3) is consistent with a direct effect of the CheZ-I21T substitution on the linker/C-helix. The fluorescence emission maximum of badan shifts to higher wavelengths as the polarity of its environment increases (44), suggesting that CheZ-I21T puts the C-helix in a more hydrophobic environment than in the wild type derivative, possibly indicative of an additional interaction. The enzyme kinetic features of CheZ-I21T were qualitatively similar to another gain of function mutant, CheZ-R54C (22), which also displays enhanced activity at low CheYp concentrations. Therefore, CheZ-I21T, CheZ-R54C, and perhaps other gain of function mutants may share an enhanced rate of association with CheYp. The clustering of these substitutions on the non-hairpin end of the four-helix bundle may implicate this region in regulation of the rate of CheYp association.

Prediction of CheZ Occupancy with CheYp—Our enzyme activity measurements were made at a CheZ concentration (50 nM) that is significantly lower than that found in the cell, which ranges from 2 to 20 μM CheZ monomer and 5 to 50 μM CheY depending on cell type and growth conditions (12, 36). Local concentrations of CheZ and CheYp are likely higher at the cell pole where the CheA kinase and much of the CheZ is localized.

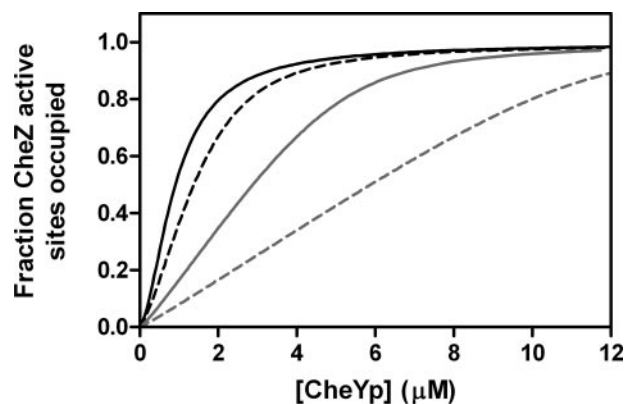


FIGURE 8. Computer predictions of CheZ occupancy. For each CheZ concentration simulations were performed to determine solely the CheZ-catalyzed phosphate release rate as a function of total CheYp concentration (the total of free CheYp and the amount bound to CheZ) for initial CheY concentrations from 0 μM in increments of 1 μM (0.1 μM for 50 nM CheZ). Solid black line, 50 nM CheZ; dashed black line, 1 μM CheZ; solid gray line, 4 μM CheZ; dashed gray line, 10 μM CheZ. The simulation for 50 nM CheZ gave a Hill coefficient of 1.7.

Simulations using the optimized kinetic constants (Fig. 7) predicted that the $K_{0.5}$ value (the concentration of CheYp that gives half the maximal velocity) increases markedly with CheZ concentration (Fig. 8). Whereas the intracellular CheZ monomer:CheY ratio appears to be fairly constant at $\sim 1:2.4$ (36), the ratio of CheZ to total CheYp is less certain but computer simulations have predicted ratios ranging from $\sim 1:1$ to $2:1$ (CheZ chain:CheY) during chemotaxis, depending on the stimulation state of the cell (38). Taking this estimation with the predictions of CheZ occupancy shown in Fig. 8 implies that CheZ would be subsaturated with CheYp under much of the window of CheYp concentrations expected during chemotaxis. This conclusion is consistent with the successful application of whole cell FRET between fluorescently labeled CheZ and CheYp as a monitor of intracellular CheYp concentrations (15, 45). The simulation further predicts that the pool of CheYp bound to CheZ may be a significant fraction of total intracellular CheYp.

Acknowledgments—We thank Doug Whitfield for construction of the plasmid encoding CheZ-I21T/F214C and Yael Pazy and Karen Lipkowitz for thoughtful review of the manuscript.

REFERENCES

1. Wadhams, G. H., and Armitage, J. P. (2004) *Nat. Rev. Mol. Cell. Biol.* **5**, 1024–1037
2. Sourjik, V. (2004) *Trends Microbiol.* **12**, 569–576
3. Bourret, R. B., and Stock, A. M. (2002) *J. Biol. Chem.* **277**, 9625–9628
4. Szurmant, H., and Ordal, G. W. (2004) *Microbiol. Mol. Biol. Rev.* **68**, 301–319
5. Turner, L., Ryu, W. S., and Berg, H. C. (2000) *J. Bacteriol.* **182**, 2793–2801
6. Berg, H. C., and Brown, D. A. (1972) *Nature* **239**, 500–504
7. Cluzel, P., Surette, M., and Leibler, S. (2000) *Science* **287**, 1652–1655
8. Boesch, K. C., Silversmith, R. E., and Bourret, R. B. (2000) *J. Bacteriol.* **182**, 3544–3552
9. Sanna, M. G., and Simon, M. I. (1996) *J. Bacteriol.* **178**, 6275–6280
10. Lovdok, L., Kollmann, M., and Sourjik, V. (2007) *J. Biotechnol.* **129**, 173–180
11. Huang, C., and Stewart, R. C. (1993) *Biochim. Biophys. Acta* **1202**, 297–304
12. Scharf, B. E., Fahrner, K. A., and Berg, H. C. (1998) *J. Bacteriol.* **180**, 5123–5128

13. Cantwell, B. J., Draheim, R. R., Weart, R. B., Nguyen, C., Stewart, R. C., and Manson, M. D. (2003) *J. Bacteriol.* **185**, 2354–2361
14. Sourjik, V., and Berg, H. C. (2000) *Mol. Microbiol.* **37**, 740–751
15. Vaknin, A., and Berg, H. C. (2004) *Proc. Natl. Acad. Sci. U. S. A.* **101**, 17072–17077
16. Rao, C. V., Kirby, J. R., and Arkin, A. P. (2005) *Phys. Biol.* **2**, 148–158
17. Lipkow, K., Andrews, S. S., and Bray, D. (2005) *J. Bacteriol.* **187**, 45–53
18. Zhao, R., Collins, E. J., Bourret, R. B., and Silversmith, R. E. (2002) *Nat. Struct. Biol.* **9**, 570–575
19. Lee, S. Y., Cho, H. S., Pelton, J. G., Yan, D., Henderson, R. K., King, D. S., Huang, L., Kustu, S., Berry, E. A., and Wemmer, D. E. (2001) *Nat. Struct. Biol.* **8**, 52–56
20. Lukat, G. S., Stock, A. M., and Stock, J. B. (1990) *Biochemistry* **29**, 5436–5442
21. Stock, A. M., Martinez-Hackert, E., Rasmussen, B. F., West, A. H., Stock, J. B., Ringe, D., and Petsko, G. A. (1993) *Biochemistry* **32**, 13375–13380
22. Blat, Y., Gillespie, B., Bren, A., Dahlquist, F. W., and Eisenbach, M. (1998) *J. Mol. Biol.* **284**, 1191–1199
23. Silversmith, R. E., Smith, J. G., Guanga, G. P., Les, J. T., and Bourret, R. B. (2001) *J. Biol. Chem.* **276**, 18478–18484
24. Silversmith, R. E. (2005) *Biochemistry* **44**, 7768–7776
25. Hess, J. F., Bourret, R. B., and Simon, M. I. (1991) *Methods Enzymol.* **200**, 188–204
26. Rathlev, T., and Rosenberg, T. (1956) *Arch. Biochem. Biophys.* **65**, 319–339
27. Smith, J. G., Latiolais, J. A., Guanga, G. P., Pennington, J. D., Silversmith, R. E., and Bourret, R. B. (2004) *Mol. Microbiol.* **51**, 887–901
28. Boxrud, P. D., Fay, W. P., and Bock, P. E. (2000) *J. Biol. Chem.* **275**, 14579–14589
29. Sheridan, R. C., McCullough, J. F., and Wakefield, Z. T. (1972) *Inorg. Synth.* **13**, 23–26
30. Sanna, M. G., and Simon, M. I. (1996) *J. Biol. Chem.* **271**, 7357–7361
31. Silversmith, R. E., Guanga, G. P., Betts, L., Chu, C., Zhao, R., and Bourret, R. B. (2003) *J. Bacteriol.* **185**, 1495–1502
32. Guhaniyogi, J., Robinson, V. L., and Stock, A. M. (2006) *J. Mol. Biol.* **359**, 624–645
33. Janin, J. (1997) *Proteins* **28**, 153–161
34. Lukat, G. S., Lee, B. H., Mottonen, J. M., Stock, A. M., and Stock, J. B. (1991) *J. Biol. Chem.* **266**, 8348–8354
35. Sanna, M. G., Swanson, R. V., Bourret, R. B., and Simon, M. I. (1995) *Mol. Microbiol.* **15**, 1069–1079
36. Li, M., and Hazelbauer, G. L. (2004) *J. Bacteriol.* **186**, 3687–3694
37. Kollmann, M., Lovdok, L., Bartholome, K., Timmer, J., and Sourjik, V. (2005) *Nature* **438**, 504–507
38. Lipkow, K. (2006) *PLoS Comput. Biol.* **2**, e39
39. Almogy, G., Stone, L., and Ben-Tal, N. (2001) *Biophys. J.* **81**, 3016–3028
40. Monod, J., Wyman, J., and Changeux, J. P. (1965) *J. Mol. Biol.* **12**, 88–118
41. Thompson, J. R., Bell, J. K., Bratt, J., Grant, G. A., and Banaszak, L. J. (2005) *Biochemistry* **44**, 5763–5773
42. Blat, Y., and Eisenbach, M. (1996) *Biochemistry* **35**, 5679–5683
43. McEvoy, M. M., Bren, A., Eisenbach, M., and Dahlquist, F. W. (1999) *J. Mol. Biol.* **289**, 1423–1433
44. Hammarstrom, P., Owenius, R., Martensson, L. G., Carlsson, U., and Lindgren, M. (2001) *Biophys. J.* **80**, 2867–2885
45. Sourjik, V., and Berg, H. C. (2002) *Proc. Natl. Acad. Sci. U. S. A.* **99**, 123–127